

Multi-objective optimization of a radial compressor impeller with subsequent robustness evaluation

T. Wanzek^{1*}, D. Karschnia¹, F. Seifert¹, J. Jasper¹, S. Rothgang¹
K. Cremanns², H. Lehmkuhl², D. Roos²

¹ KSPG AG, Neuss, Germany

² Institute of Modelling and High-Performance Computing (IMH), Niederrhein University of Applied Sciences, Krefeld, Germany

Summary

Downsizing has become an important measure to meet the increasing demand for fuel-economy in the automotive industry. In this context the KSPG AG develops an electrically driven radial compressor (electrical Air Compressor = eAC).

In a cooperation project of KSPG AG and the IMH a high dimensional, multi-objective design optimization of the fluid mechanical and structural properties of the eAC impeller was carried out. The underlying CAE-process consists of a proprietary KSPG Excel Tool to describe the rotor geometry and the ANSYS Workbench to build up a CAE-model of the impeller structural and fluid mechanics. The whole process is controlled by optiSLang.

In the first step a sensitivity analysis of a total of 49 input parameters and 49 output parameters was conducted. Based on this sensitivity analysis metamodels were used to do a global, multi-objective optimization considering all input parameters. In continuation an optimization using real solver runs was performed for the sensitive parameters in the relevant parameter subspace. Finally an estimation of the failure probability based on assumed distributions of the input parameters was provided for the optimized design.

The key outcome of the optimization was a significant reduction of the mass and moment of inertia of the impeller and an improved efficiency and pressure ratio near the surge line. Last but not least the optimized impeller design proves to be robust against statistical variation of selected input parameters.

Keywords: Radial compressor impeller, Multi-Objective Design Optimization, Automotive

* Kontakt: Tim Wanzek, KSPG AG, Alfred-Pierburg-Str. 1, D-41460 Neuss, tim.wanzek@de.kspg.com

1 Introduction

Downsizing and downspeeding have become important measures to meet the increasing demand for fuel-economy in the automotive industry. To increase the maximum power output per litre displacement of the engine (i.e. kW/l), the size and inertia of conventional exhaust gas turbochargers in single stage supercharged engines are increasing. This leads to a conflict of objectives between high fuel efficiency at nominal power of the engine and a good transient performance especially at low engine speeds (so called low end torque).

One measure to overcome this conflict is to use multiple stages for the supercharging of the engine. By using an electrically driven compressor, a part of the charging pressure can additionally be completely decoupled from the engine speed or the enthalpy stream available at the turbine. Furthermore, the tendency of automotive manufacturers to install 48 V electric systems into their cars opens up a wider range of useable power and operational scenarios for such electric superchargers. In this context, KSPG AG is developing an electrically driven radial compressor (electrical Air Compressor = eAC), which will support car manufacturers in increasing fuel efficiency and lowering emissions of their engines.

This eAC faces some restrictions that will result in a design different from the design of conventional exhaust gas turbocharger compressor stages with the same requirements regarding mass flow and pressure ratio. First of all, the maximum speed of compressor is limited due to different limitations on the drive side of the eAC. Hence, the eAC has to operate at comparably low specific speeds ($N_s > 0.5$) with a large rotor diameter. To keep the rotor diameter as small as possible, the blade discharge angles have to be very small and the flow incidence angles and the absolute Mach number at the outlet are comparably high.

A second restriction in this application is the limited design space available for the eAC. In combination with the large impeller diameter, the space available for the radial diffuser is very limited. Despite that, the recovery of static pressure inside the diffuser has to be maximized to keep the losses inside the volute low.

The third challenge is the transient performance of the eAC itself. To ensure an immediate buildup of the boost pressure, the eAC has to be able to accelerate from zero to maximum speed in significantly less than 0.5 s. To reach this goal, the moment of inertia of the complete rotor assembly including the impeller has to be as low as possible. This conflicts with the need for a large rotor diameter due to the limited speed of the electric motor.

Due to these special requirements, finding a perfectly suited eAC design based only on well-known design guidelines is very challenging. Hence the eAC was found to be a good example to apply multidisciplinary and multi-objective numerical optimization at KSPG AG. The availability of very well parameterized eAC geometry provided by a proprietary design tool developed at KSPG AG, as well as the fact that required simulation models are comparably simple in terms of geometry and physical models, confirm the ability to apply the numerical optimization methods mentioned above.

Another goal of this project was to set a starting point in robustness evaluation as a first step towards complete Robust Design Optimization (RDO). In order to achieve fast progress and good results the project was conducted in close collaboration with Institute of Modelling and High-Performance Computing (IMH) in Krefeld. The scope of the project was the following:

- Prepare the geometry and simulation model for the use in a numerical optimization process.

- Conduct a Design of Experiments under variation of all available parameters.
- Perform a sensitivity analysis for the attained data and create appropriate metamodels.
- Carry out global pre-optimization based on the metamodel followed by local optimization of most sensitive parameters using real solver runs.
- Evaluate the general robustness of the optimal design against assumed statistical variation of selected input parameters.

2 Simulation model and workflow definition

The whole optimization process is based on an Excel-tool, which is able to describe the geometry of the impeller by a maximum of 79 parameters. In addition to the general dimensions of the impeller it uses Bezier-splines to describe the different characteristics, such as meridional contour, blade angle or blade thickness distribution. This data is used to calculate a point based description of the different parts of the impeller surface, i.e. the wheel body, main blade and splitter blade. Additionally, points and curves needed to create the fluid volume of one channel of the impeller including inflow and radial diffuser are created. This data is exported to different ASCII-files for further processing.

In the next step the ASCII-files are imported as point and curve data into ANSYS DesignModeler within ANSYS Workbench. Therein, they are transformed into curves, surfaces and volume bodies which form the final solid model of the impeller wheel and the fluid channel used for the CFD-analysis (see

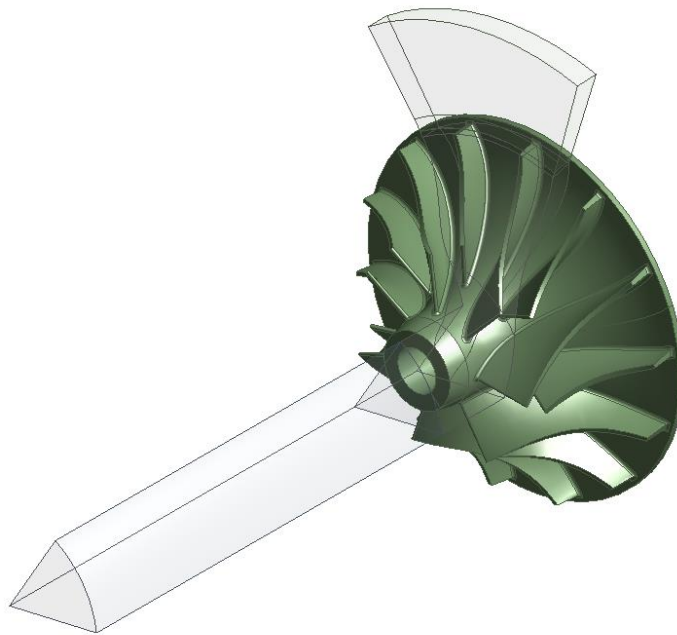


Figure 1: Solid (green) and fluid volume model (transparent) as created by ANSYS DesignModeler.

The fluid volume is meshed by ANSYS Meshing with the use of tetrahedrons and prism layers near walls to ensure sufficient resolution of the boundary layer (see Fig. 2). The resulting mesh is used for CFD simulations of two different load cases. The first load case

represents the design point and the second, the operation near the surge line of the compressor.

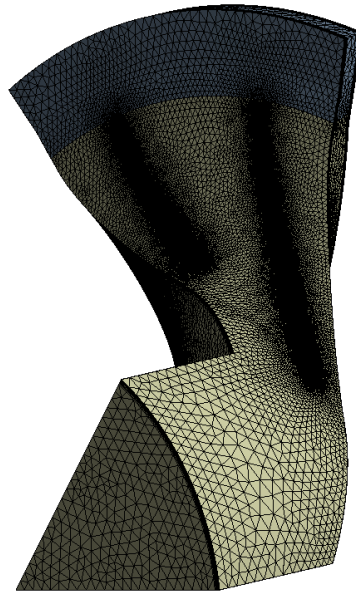


Figure 2: Volume mesh of periodic flow channel for CFD analysis.

The solid model is used in a static structural analysis to calculate the stresses prevailing on different parts of the rotor at maximum rotational speed. In addition, a modal analysis is carried out in order to determine the first four eigenmodes of the structure.

The simulations result in 49 responses in total, that are available in the parameter set of ANSYS Workbench. They consist of 32 results of the CFD simulations such as total and static pressure ratios, compression efficiency and axial force acting on the impeller and 17 results derived from the FEA calculations such as equivalent stresses, eigenfrequencies, mass and moment of inertia of the rotor. In addition to these scalar responses, a vector consisting of iteration number and total pressure ratio is exported to a csv-file from CFD-Post via a session file in order to judge the convergence of the CFD calculations.

The complete workflow, including input and output parameters of optiSLang as well as the interfaces to the linked software, is displayed in Fig. 3. Dynardo optiSLang controls the whole CAE-process that is mandatorily fully automated. The process works as follows: optiSLang defines a new design which consists of a complete set of input parameters varied within their limits. The geometry parameters linked to the Excel-based design tool are pasted into the Excel-file, the geometry definition is updated and the new ASCII-files are exported by executing a Visual Basic (VBA)-macro. In the next step the Workbench-project template is opened and the parameters defined here are updated. Afterwards a python-script is called that first updates the file links to the geometry ASCII-files inside DesignModeler and then performs a complete Workbench project update. Afterwards, the scalar results are directly exported to optiSLang whereas the vectors of the convergence history are exported by a separate python script which opens CFD-Post and executes the previously described session file. In a last step, the signal processing capabilities of optiSLang are used to derive the coefficient of variation (CoV) from the convergence history data.

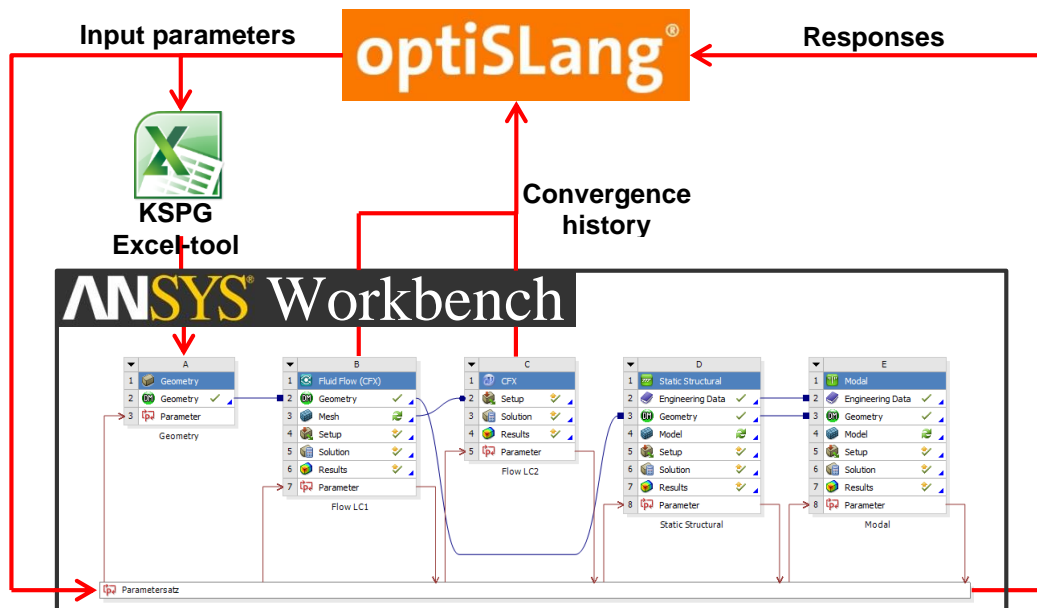


Figure 3: Diagram of the CAE-process controlled by optiSLang.

3 Sensitivity analysis and metamodel of optimal prognosis

After the description of the model and CAE process, the following parts describe a common procedure for a multidisciplinary and multi-objective numerical optimization following a robustness evaluation.

Fig. 4 summarizes the necessary steps for the optimization.

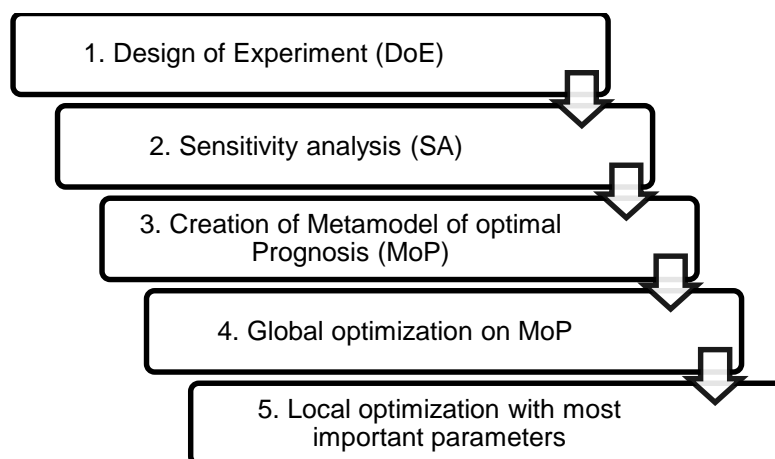


Figure 4: Steps for a multidisciplinary and multi-objective numerical optimization.

The aspired multidisciplinary and multi-objective numerical optimization including first steps towards RDO, is based in the first step on a valid design of experiment (DoE), which is followed by a sensitivity analysis. Since latin hypercube sampling (LHS) overcomes disadvantages of sampling in terms of correlation and uniformity of sample distribution

(compare, for example, Plain Monte Carlo sampling) [4], it was chosen as the appropriate DoE method for the present task. A total of 130 designs were calculated within the DoE. Some pre work was necessary to establish model stability, which was finally good: only 17 designs of the sampling (< 15%) failed. Model stability is a common difficulty in dealing with parametric CAE models.

Reasons for failed designs were:

- The geometry could not be regenerated.
- Mesh in mechanical, modal or CFD analysis could not be regenerated.
- Solver failed in mechanical or CFD analysis.

Once model stability has been established, it is recommended that a plausibility check is performed on the succesful designs. Depending on the physics taken into account, there are different possibilities for verifying the results. In this case, one part (in addition to anthill plots) of the plausibility check was the analysis of the convergence of the CFD-analysis by examining the coefficient of variation (CoV) as introduced in section 2:

$$\text{CoV} = \frac{\text{Standard deviation}}{\text{mean value}} \quad (1)$$

Calculation of the CoV refers to only the last 50 of in total 300 iterations of the CFD analysis. The maximum allowed CoV was 0.3%. Fig. 5 shows an example of the CoV for the pressure ratio. The green line shows the reference design. The red lines represent designs which have a CoV > 0.3%.

A further plausibility check is provided by the analysis of output anthill plots. They also show non-feasible behavior. An example is shown in Fig. 6, where it is clearly apparent that design 13 is an outlier compared to all other designs.

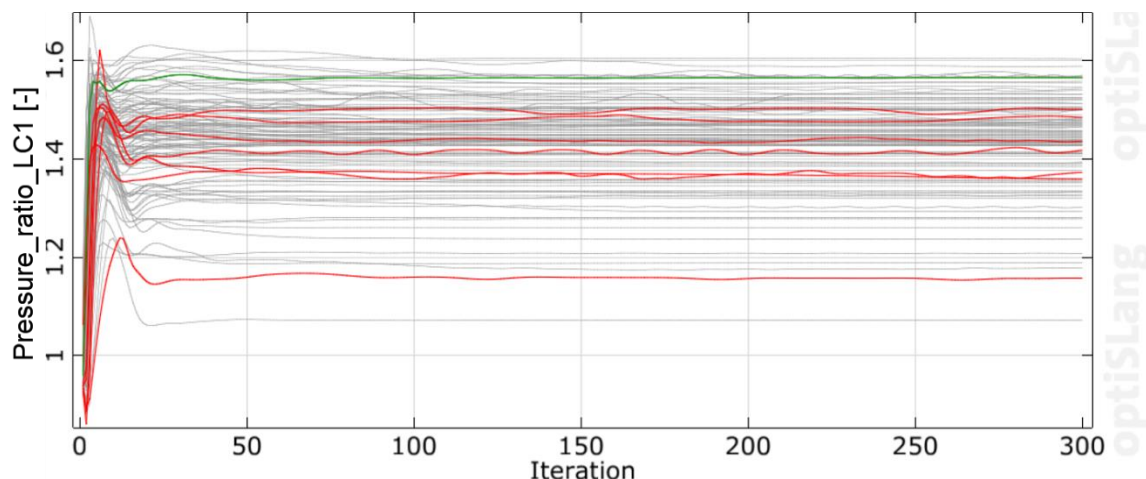


Figure 5: Cov plot of the Pressure_ratio_LC1. Red: CoV>0.3%, green: reference design.

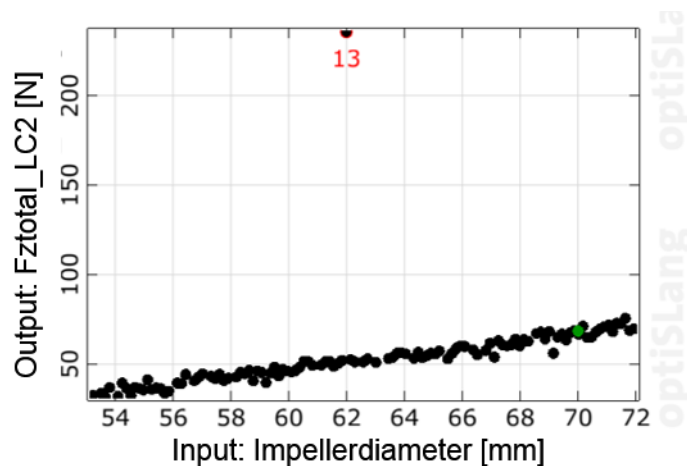


Figure 6: Anthill plot of output parameter Fztotal.

After all outputs had been checked regarding plausibility, 12 additional designs were removed from the DoE. Thus, the success rate of samples was reduced, but was still at a level of 78%. A reduced success rate always results in unwanted input correlations, which adversely affect the statistical measures. Other projects [5], [6] have shown that 78% is still an acceptable level. One method that helps to prove that the input space is still sufficiently covered is to check the minimum and maximum values which occur in the DoE for a specific input parameter. For example, the rotation speed for the load case LC1 should be between 6618 rad/s and 8990 rad/s. Fig. 7 shows that the coverage in the DoE is still good due to the achieved range of 6624 rad/s to 8904 rad/s. Because 29 of 130 designs failed or were removed from the DoE, the initial uniform distribution of the input parameters was affected but the input correlation was still $<10\%$, which was regarded as an acceptable rate.

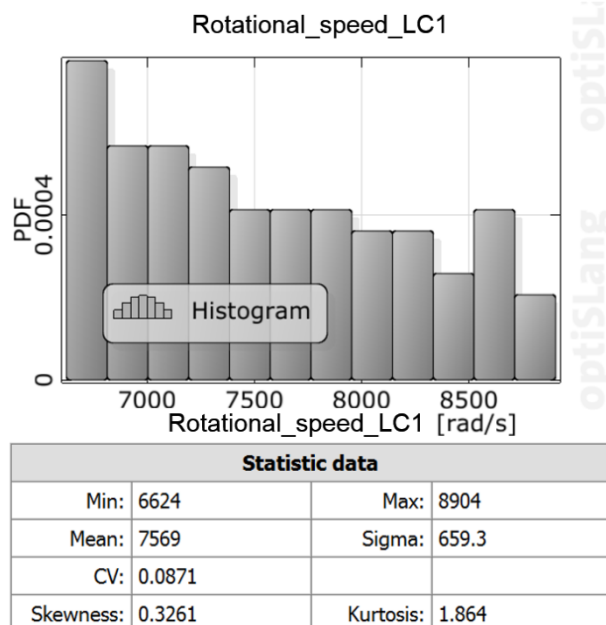


Figure 7: Histogram of the dependent parameter rotational_speed_LC1.

4 Sensitivity analysis and metamodel of optimal prognosis

In the optimization workflow, the plausibility check is followed by the sensitivity analysis and the creation of the metamodels for each response. In total 49 geometrical input parameters, which are an excerpt of the 79 parameters included in the parametric eAC-impeller model defined by the Excel-tool, are available. Not all of the 49 parameters are important for each output parameter or for the corresponding metamodel. Parameters which have no significant influence on a specific output reduce the prognosis quality of the corresponding metamodel because they cause additional noise in the output. Therefore it is necessary to reduce the parameter space for each output by only taking the most important parameters into account for metamodeling. A further benefit of reducing parameter space for each output is a faster convergence of the algorithm in the local optimization (after global optimization) and maybe also an increased chance of finding better results than would be possible with all parameters. Nevertheless, before the local optimization, a first step of global optimization with all parameters used in the metamodel is necessary since parameters with a very small influence could also contribute to a better result. This is especially the case if there are a lot of parameters with small influence. The reduction of the parameter set through the identification of important input parameters for each specific output is part of the sensitivity analysis in optiSLang.

The objectives of a sensitivity analysis are summarized as:

- Identification of sensitive parameters and their influence on the various outputs, objectives of optimization and constraints.
- Reduction of the parameter space for the optimization.
- Analysis of correlations between input parameters and output parameters. (Which change of an input variable has a positive or negative effect on an output?)
- Estimation of the most important variables for the metamodels for the respective output variables.
- Determination of the prognosis quality of the metamodels.

To estimate the prognosis quality of the metamodel, optiSLang introduced the so-called coefficient of prognosis (CoP) [7]. $CoP = 1$ denotes the best possible prognosis quality of the metamodel and $CoP = 0$ denotes the worst. A high CoP also means that all correlation between the input parameter and the specific output parameter has been found. An example of the optiSLang result is shown in Fig. 8. On the left side, the response surface of the metamodel dependent on the two most important input parameters is shown. On the right side, the five most important parameters for the output Efficiency_LC1_Norm are displayed. The total CoP for output Efficiency_LC1_Norm is 73%. This indicates that not all correlations between the inputs and the output have been found. The single CoPs for each input parameter show their contribution to the output and hence provide a ranking of the most important parameters. Since the sum of the single CoPs is higher than the overall CoP ($84\% > 73\%$), multivariate dependencies of input parameters are present [7].

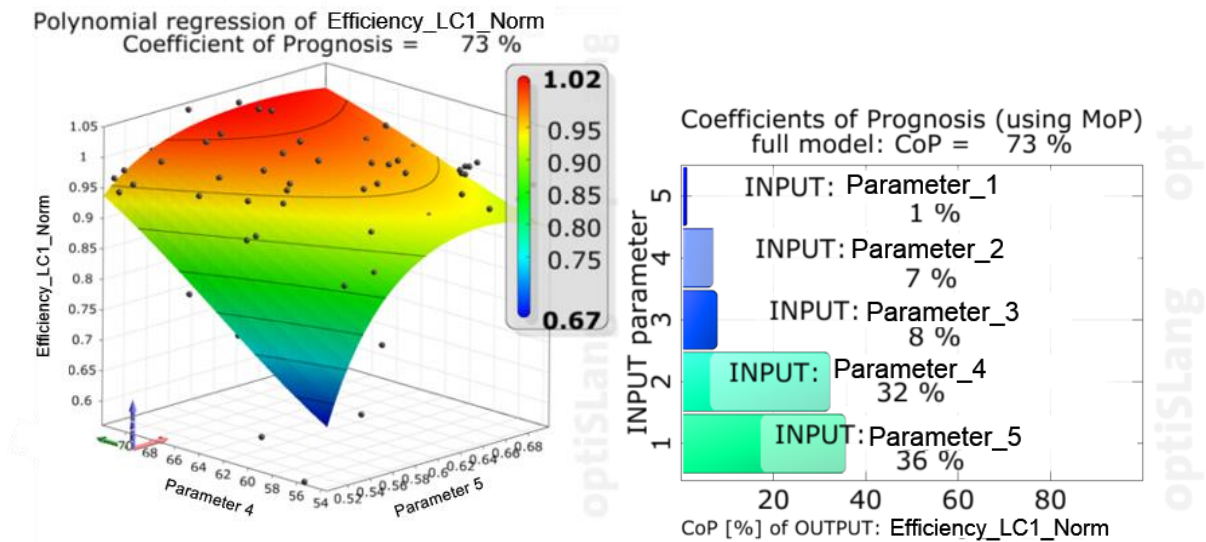


Figure 8: Example of a metamodel for the output Efficiency_LC1_Norm.

Poor metamodels can occur if the specific outputs result in very complex or even discontinuous behavior. Discontinuity can appear if, for example, the point of highest stress in a FE-analysis results in different positions for different design points. This leads to poor metamodels and hence to low CoP values in most cases. Non-convergent results of the CFD analysis can lead to such problems, too. Therefore the issue of output complexity and discontinuity has also been addressed in the result check - described in Section 3. An example for discontinuous behaviour of output is shown in Fig. 9. It shows the first eigenfrequencies of the geometry for the different designs calculated. There appears to be a switch between the local and global eigenfrequencies in different designs, which leads to a low CoP value.

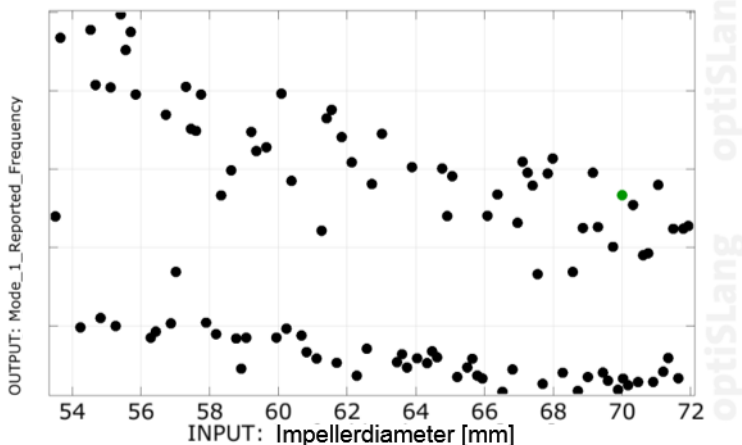


Figure 9: Example of a metamodel for the output Efficiency_LC1_Norm.

An overview of all output parameters which are used for the definition of the optimization objectives and their corresponding CoP values are given in Table 1. All CoPs except the CoP of Stat_pressure_ratio_LC1_norm are very good (CoP > 90%) or acceptable (90% < CoP < 70%). So there are some deviations expected in the Stat_pressure_ratio_LC1_norm, when comparing the result of optimization (on metamodel) to the validation result from the CFD run recalculation.

For the local optimization which was performed in a second optimization step, the most important input parameters were reduced to a total number of six. These are the most important input parameters for all optimization objectives.

Output Parameter	CoP	Annotation
N1: Efficiency_LC1_Norm	0.73	Total isentropic efficiency of load case 1 normalized on the reference design
N2: Stat_pressure_ratio_LC1_Norm	0.50	Static pressure ratio of load case 1 normalized on the reference design
N3: Efficiency_LC2_Norm	0.90	Total isentropic efficiency of load case 2 normalized on the reference design
N4: Stat_pressure_ratio_LC2_Norm	0.75	Static pressure ratio of load case 2 normalized on the reference design
N5: Bending_moment_Norm	0.95	The bending moment of the eAC-impeller normalized on the reference design
N6: Moment_of_inertia_Norm	0.98	The moment of inertia of the eAC-impeller normalized on the reference design

Table 1: Overview CoPs of all output parameters used for definition of the optimization objectives.

5 Global and local optimization

The optimization is performed in two steps. In the first step, a global pre-optimization is carried out on the metamodel of optimal prognosis taking all input parameters (unimportant and important) into account. In the second step, a local optimization is performed by starting from the best design of pre-optimization. The procedure is summarized in Fig. 10.

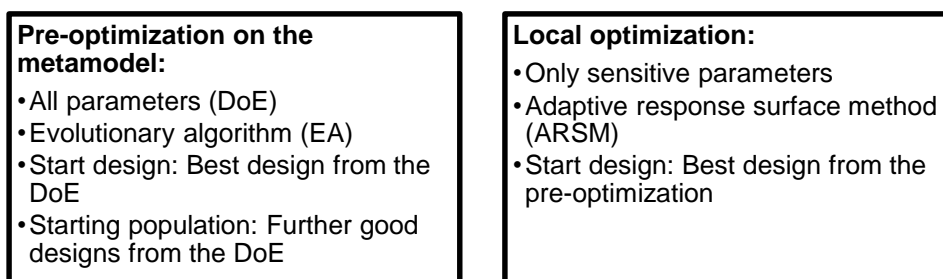


Figure 10: Optimization procedure.

The aim of the optimization is to minimize an objective function under specific constraints:

$$f(x_1, x_2, \dots, x_N) \rightarrow \text{Min} \quad (2)$$

The variables (x_1, x_2, \dots, x_N) are the N input parameters of the optimization problem. The range of these variables is specified by lower and upper limits. In the current case, the boundaries of the optimization parameters correspond to the limits defined for the DoE. The objective function is composed of multiple terms.

The difficulty in defining the objective function is linked to the challenge of combining objectives in terms of fluid mechanical and structural mechanical performance variables. The dominance of a single target in the optimization process should be avoided. Therefore the responses used for the objective function are normalized by the corresponding values of the reference design. Additionally, different objective weights were tested in order to reduce dominant behavior of specific outputs in the objective function. After several iterations the following objective function was defined:

For CFD:

$$\max(O1 = (0.4 * (0.7 * N1 + 0.3 * N2) + 0.6 * (0.3 * N3 + 0.7 * N4))) \quad (2)$$

For mechanic:

$$\min(O2 = (0.7 * N5 + 0.3 * N6)) \quad (3)$$

Overall optimization objective:

$$\min(O3 = (-0.7 * O1 + 0.3 * O2)) \quad (4)$$

In addition to the objective function, a total of 14 constraints are defined for the optimization runs:

- Global stress maximum of all defined stress outputs should be lower than the maximal allowed stress value
- Minimal pressure ratio should be higher than a specified value
- Maximal deformation should be smaller than a specified value
- First eigenfrequency should avoid a critical range which corresponds to the machine frequency
- Minimal impeller diameter should be higher than a specific value
- Diffuser diameter should also be higher than a specific value

In the first step, the global optimization evaluated 4000 designs on the metamodel. Fig. 1 shows the convergence of the optimization algorithm. Fig. 2 shows the convergence of the pressure ratio of the best design 3943 (red line). Even a recalculation of the best design using the ANSYS simulation model shows a really good match with the approximated result on the metamodel as shown in Table 2. This is further evidence to prove the prognosis quality of the metamodel. The ability to use metamodels provides enormous time-savings compared to optimization tasks which call solver runs for each design. Table 2 also shows the results of the best design compared to the reference design.

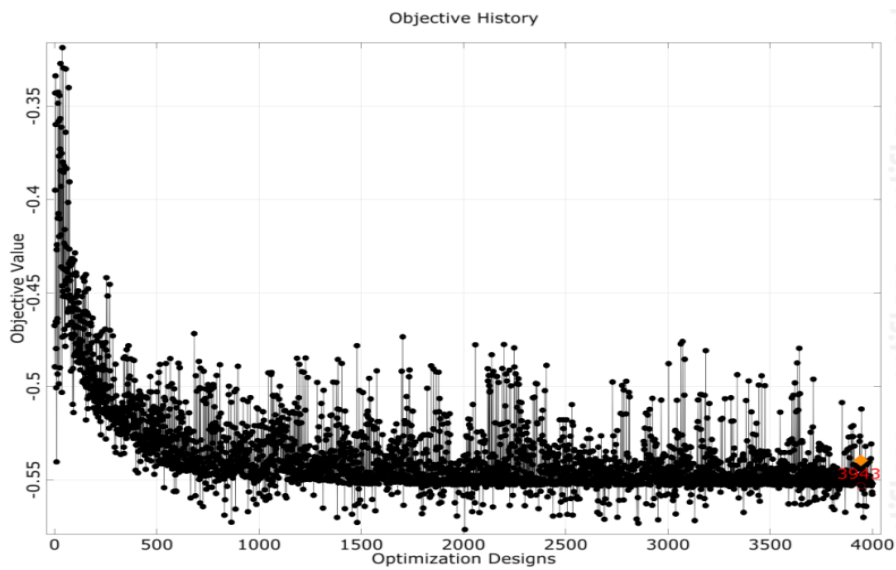


Fig. 1: Optimization progress on the metamodel.

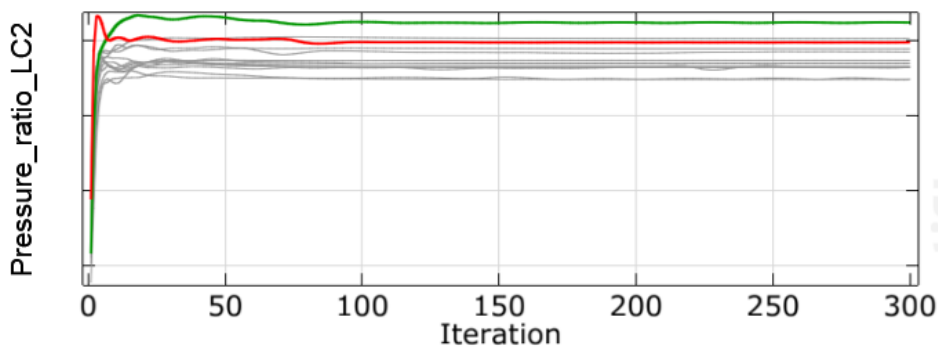


Fig. 2: Progress of the pressure ratio of load case 2 of the best design in the pre-optimization, grey lines are other designs from the DoE, green line = initial design.

Output / Objective (term)	Reference	Design 3943 MoP/Calculated	Difference to reference in %
N1: Efficiency_LC1_Norm	1.00	1.02 / 1.00	+0.1
N2: Stat_Pressure_ratio_LC1_Norm	1.00	1.02 / 0.98	-1.6
N3: Efficiency_LC2_Norm	1.00	1.04 / 1.03	+2.7
N4: Stat_Pressure_ratio_LC2_Norm	1.00	1.01 / 1.01	+1.2
N5: Bending_moment_Norm	1.00	0.53 / 0.50	-50.2
N6: Moment_of_inertia_Norm	1.00	0.54 / 0.58	-42.1
O1: CFD	-1.00	-1.02 / -1.01	+0.8
O2: Mechanic	1.00	0.54 / 0.55	-44.7
O3: Overall	1.00	-0.55 / -0.54	-46.1

Table 2: Overview of the preoptimization on the metamodel with best design 3943.

The results show that the pre-optimization achieved a huge improvement of -44.7% for the mechanical objective which resulted in a decrease of the bending moment and the moment of inertia. There is only a small improvement of 0.8% for the CFD objective. The efficiency is comparable to the reference design. The same can be seen for the pressure ratios. Fig. 1 indicates that the global optimum was found, because from iteration 1500 onwards, the global level of the objective function is fixed and so no further major improvements in the local optimization can be expected.

Fig. 3 shows the pressure contour at a span ratio of 0.5 of the reference design and the preoptimized design 3943 respectively. It can be seen that the pressure distribution is more uniform for the preoptimized design than for the reference design.

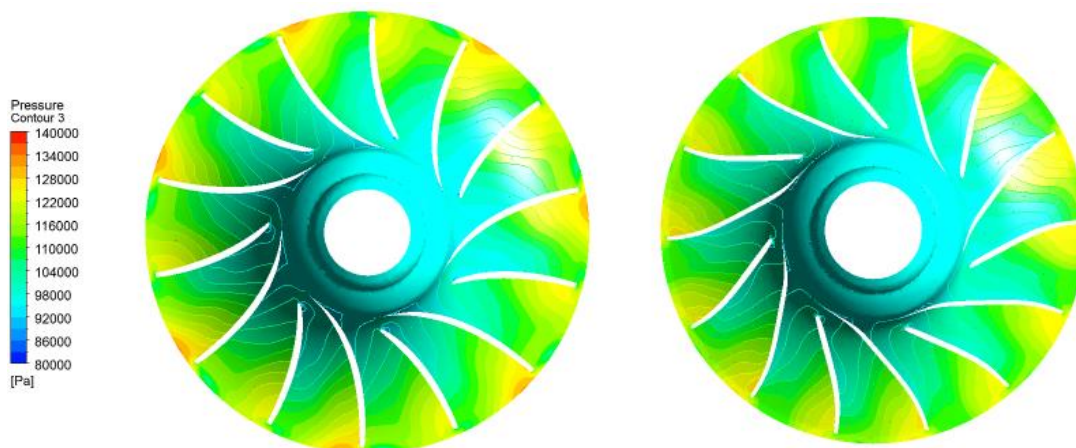


Fig. 3: Comparison of pressure contour at span ratio 0.5 of reference design (left) and preoptimized design (right).

In the second step of optimization design 3943 was used as the start design for local optimization. By the end, 175 designs had been calculated with an adaptive response surface optimization algorithm (ARSM) calling ANSYS simulation model solver runs. Fig. 4 shows

the convergence progress of the local optimization. It shows fast convergence due to limited availability of optimization potential.

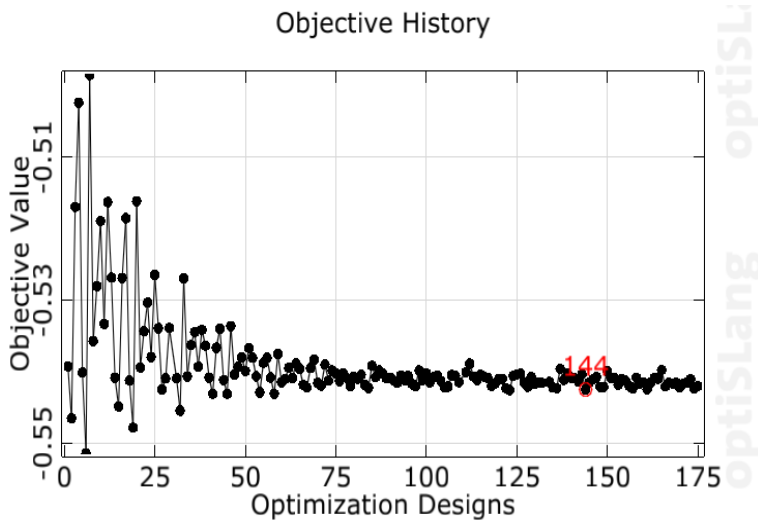


Fig. 4: Objective history for the local optimization

Output / Objective (term)	Reference	Design 144	Difference to reference in %	Difference to preoptimization in %
N1: Efficiency_LC1_Norm	1.00	1.00	+0.3	+0.2
N2: Stat_Pressure_ratio_LC1_Norm	1.00	0.98	-2.5	-0.9
N3: Efficiency_LC2_Norm	1.00	1.03	+2.5	-0.2
N4: Stat_Pressure_ratio_LC2_Norm	1.00	1.01	+1.3	+0.0
N5: Bending_moment_Norm	1.00	0.48	-51.8	-3.3
N6: Moment_of_inertia_Norm	1.00	0.57	-43.0	-1.5
O1: CFD	-1.00	-1.01	-0.7	-0.1
O2: Mechanic	1.00	0.54	-45.6	-1.6
O3: Overall	1.00	-0.54	-45.8	-0.6

Table 3: Overview of the results of the local optimization with best design 144.

Table 3 shows the results of the best design 144 for local optimization. The optimization achieved a further small improvement for the mechanical objective of 1.6% and even lost some points for the CFD objective (0.1%). The overall objective reached an improvement of 0.6% compared to the 46.1% in the preoptimization. Fig. 5 shows the comparison of the pressure contour at a span ratio of 0.5 of the local and global optimization.

In summary, the optimization resulted in a significant improvement especially in the mechanical objective (-45.6%) and a slight improvement in the CFD objective (-0.7%) while maintaining the efficiency level. The local optimization in the sensitive subspace showed only minor changes compared to the preoptimization (overall objective -0.55%). The mass of the impeller could be reduced significantly to -35% compared to the reference design.

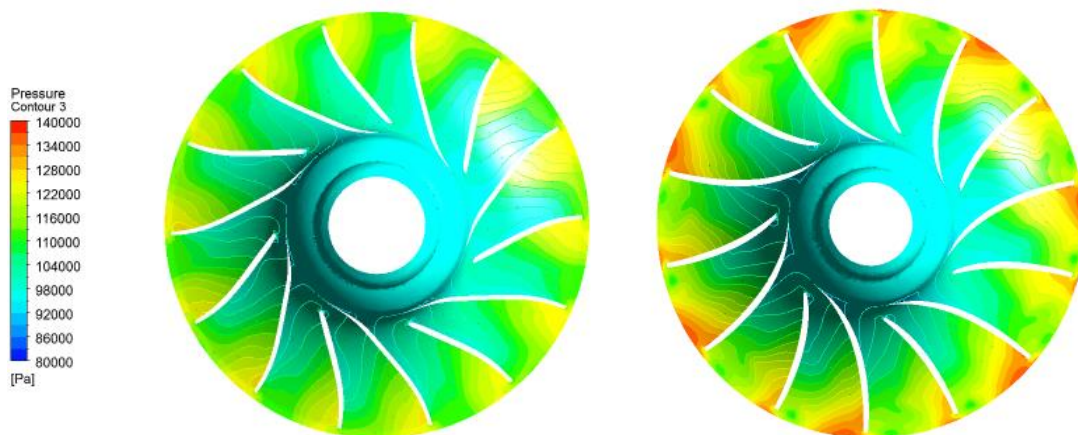


Fig. 5: Comparison of pressure contour at span ratio 0.5 of preoptimized design (left) and optimal design (right).

6 Robustness evaluation

Finally, a robustness evaluation for the optimal design 144 was performed. The robustness evaluation aims to identify the influence of scattering parameters on the performance of the optimal design. In reality, each process parameter will scatter and thus can have a significant impact on the reliability of the product (e.g. exceedance of maximum stresses or lifetime reduction) as well as on the performance (e.g. reduced efficiency). In this case, scattering of the geometry parameters (manufacturing tolerances, e.g. the impeller diameter), of the loads (e.g. massflow) and also of the material parameters (e.g. modulus of elasticity) is considered. For the robustness evaluation, optiSLang requires information regarding scattering characteristics such as the CoV and the distribution type. In practice, this information is often difficult to obtain since extensive (and often expensive) series of measurements are needed. This problem was faced in this project, too. Hence Gaussian distribution was assumed for each scattering input parameter. In addition, conservative assumptions were made for the CoV of each parameter.

The robustness analysis is comparable to the sensitivity analysis. In both cases the active input parameters are varied between their bounds in a DoE. In the case of the sensitivity analysis, these bounds are the design limits defined by the user with a uniform distribution. In the robustness analysis, the bounds are specified by their tolerances / CoV and specific distribution type. The results of the robustness analysis are analogous to the initial sensitivity analysis and address the following areas:

- Which scattering parameters have the most influence on a specific constraint (e.g. safety factor of total stress)?
- Are there correlations of scattering parameters?
- Determination of statistical data (e.g. min / max value).

In addition, probabilities for exceeding the limit state function - which means design failure - can be estimated by providing information about sigma levels.

The general approach in robustness evaluation is to start with a DoE for the scattering parameters in which the parameter limits refer, for example, to manufacturing tolerances and the reference value (= expected value) refers to the best design of optimization (in the present

approach: design 144). DoE sampling considers mandatorily the distribution type of each variable. The robustness evaluation in this project is at least a feasibility study for the application of methodology on eAC due to the lack of scatter information mentioned above. Its results should not be taken over for, for example, adjusting production processes. But the results of the robustness evaluation will provide hints about where to start with measurement series in order to register scattering characteristics.

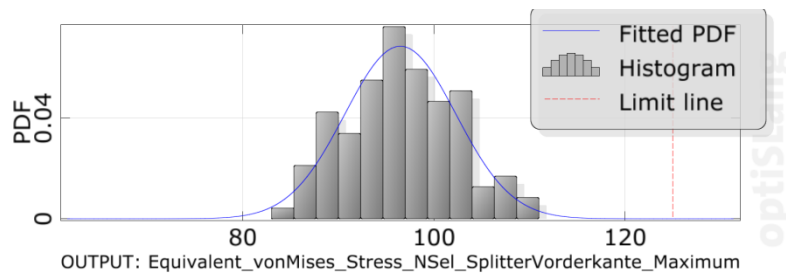
The robustness evaluation presented in this paper addresses 15 parameters (geometry, material and loads) which showed the highest impact on the optimization objective and constraints. For the 15 active parameters the settings for the expected value are derived from design 144. All other parameters are set to be constant referring also to design 144. For the active geometry parameters CoV is conservative with a value of 0.02. For the material and load parameters the CoVs are shown in Tables 4 and 5.

Parameter	Distribution type	CoV
Modulus of elasticity	Normal	0.05
Density	Normal	0.05
Poisson's ratio	Normal	0.10

Table 4: Overview of material parameters for the robustness evaluation.

Parameter	Distribution type	CoV
Massflow_LC1	Normal	0.05
Massflow_LC2	Normal	0.05

Table 5: Overview of load parameters for the robustness evaluation.



Statistic data	
Min: 83.01	Max: 111
Mean: 96.49	Sigma: 5.81
CV: 0.06021	
Skewness: 0.08799	Kurtosis: 2.599
Fitted PDF: Normal	
Mean: 96.49	Sigma: 5.81
Limit x = 125	
P_rel: 1	1 - P_rel: 0
P_fit: 1	1 - P_fit: 4.60991e-007
Sigma-Level: 4.9076	
Probability P(X<x) = 0.95	
x_rel = 106.752	x_fit = 106.044

Fig. 6: Example result for one stress output of the robustness evaluation.

Fig. 6 is an exemplary result of the robustness evaluation for one stress output. It gives information about:

- min/max and mean value of the output
- standard deviation and CoV
- user-selected distribution type for Probability Density Function (PDF) and its additional parameters (such as skewness and kurtosis)
- if a failure limit is set (in our example the limits of the optimization constraints), the probability of failure fit and relativity is given, whereby relativity is related to the histogram (number of designs which exceed the limits in the DoE) and fit corresponds to the failure probability if the given distribution type is considered.
- the possible output value if a 95%-quantil is set, i.e. the possible value for the output if a 5% probability of failure is allowed.

<i>Output</i>	<i>CoV</i>
Equivalent_vonMises_Stress_1	0.07
Equivalent_vonMises_Stress_2	0.06
Equivalent_vonMises_Stress_3	0.07
Equivalent_vonMises_Stress_4	0.06
Equivalent_vonMises_Stress_5	0.07
Equivalent_vonMises_Stress_6	0.06
Equivalent_vonMises_Stress_7	0.11
Equivalent_vonMises_Stress_8	0.10
Equivalent_vonMises_Stress_9	0.05
Penetration_Maximum	2.17
Mode_1_Reported_Frequency	0.06
p2tot_to_p1tot_LC1	0.01
Efficiency_LC1_Norm	0.01
Stat_pressure_ratio_LC1_Norm	0.01
Efficiency_LC2_Norm	0.01
Stat_pressure_ratio_LC2_Norm	0.01
Bending_moment_Norm	0.06
Moment_of_inertia_Norm	0.08

Table 6: Results of robustness evaluation.

For this stress output the limit was set to 125 MPa. The probability of failure is $4.6e-7$ (= sigma level: 4.9 if a normal distribution is assumed). So, if a failure probability of 5% is allowed, it is also possible to decrease the stress limit to 106 MPa to correspond to the 5% failure probability, which would result in a deterministically higher safety factor. In other words, the current design is “too safe” and some further changes to increase the limit of 106 MPa to 125 MPa are allowed, for example to further optimize the structural mechanic objective.

Creating a metamodel on the result of the robustness evaluation and determining the CoPs will identify the most important scattering parameter for each output. In doing so, the parameter with the highest influence on the specific outputs regarding robustness will be detected. Hence, information is available in order to reduce the CoV of output parameters efficiently. For example, information is provided on whether it is more efficient to reduce the manufacturing tolerances for a specific geometry part or to improve the material quality. Thus, the robustness analysis provides the opportunity to perform target-oriented quality improvements to the products.

The resulting CoVs of each output derived from the robustness evaluation are shown in Table 6. Ignoring CoV for output Penetration_Maximum which was caused by some non feasible max. values in the DoE, the overall maximum value for CoV is 11%. Thus, output variance correlates with the input variance (CoV of 2% - 10%). This indicates robust design behavior. In addition, for most output parameters the distribution type is in conformance with the input type which is a normal distribution (see e.g. Fig. 6). It can also be seen in Table 6 that, for the majority of outputs, the CoV is below 1 %. Fig. 7 - Fig. 10 show exemplarily that the CFD objective outputs of the optimized design (blue line) are located close to the mean value of the

robustness evaluation (grey lines) for both loadcases. This is a further indicator for a robust design.

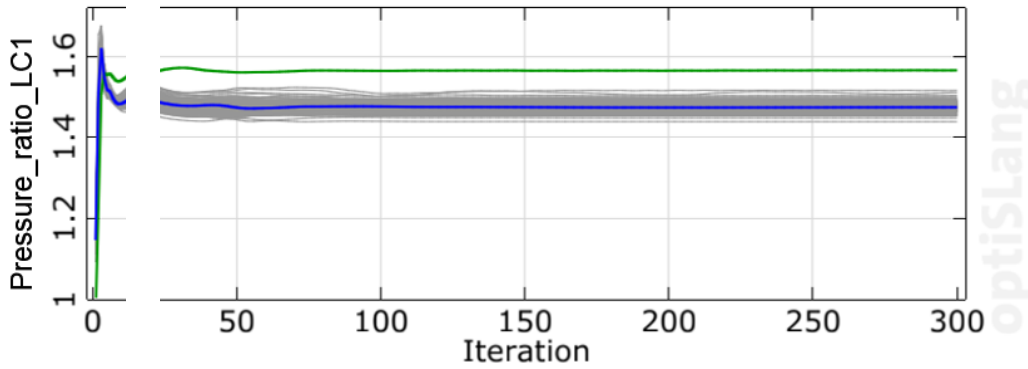


Fig. 7: Pressure ratio LC1 of the best design 144 (blue) compared to designs of robustness evaluation (grey) and reference (green).

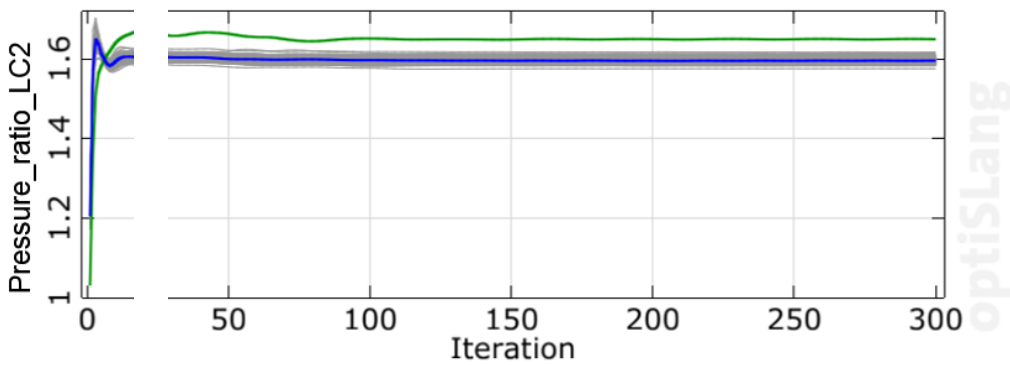


Fig. 8: Pressure ratio LC2 of the best design 144 (blue) compared to designs of robustness evaluation (grey) and reference (green).

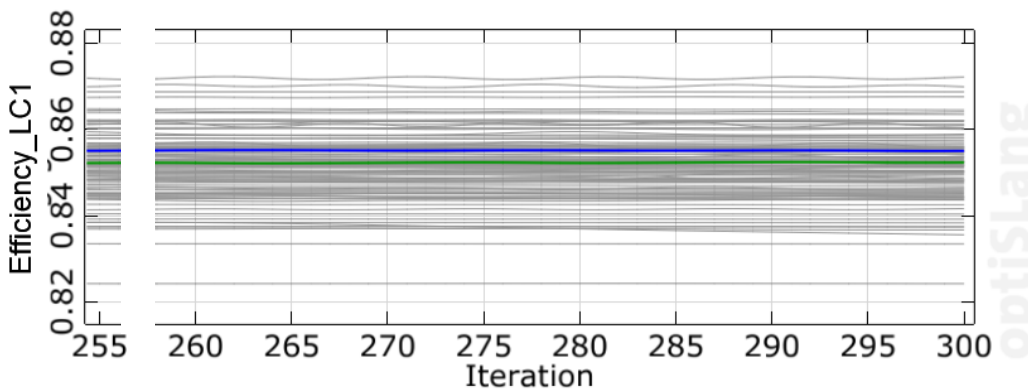


Fig. 9: Efficiency LC1 of the best design 144 (blue) compared to designs of robustness evaluation (grey) and reference (green).

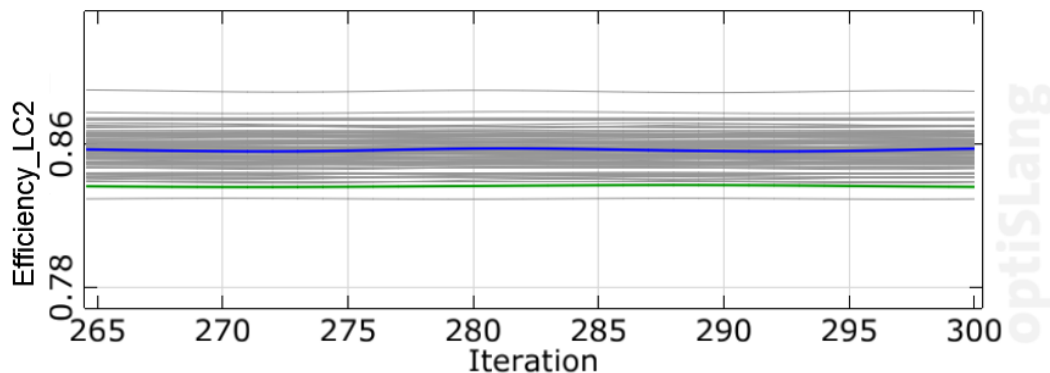


Fig. 10: Efficiency LC2 of the best design 144 (blue) compared to designs of robustness evaluation (grey) and reference (green).

Finally, the feasibility study for the application of robustness evaluation on eAC was successful. Based on the assumptions for the scattering inputs, the optimized design (design 144) shows a robust behavior, modified assumptions could lead to another result. Therefore, an investigation of those parameters which influenced the robustness evaluation results is required. That means, for example, starting with the measurement series for the real geometry, the manufacturing process, the materials used, etc.

7 Result validation

After the identification of the optimal designs, validation runs of the CFD results were performed on a numerical basis. This is necessary because the CFD-model used for the optimization only covers one flow channel of the rotor and does not contain the volute. For this purpose, the optimized impeller geometries were combined with the volute from the reference design. A comparison between the two different CFD-models is shown in Fig. 11 below.

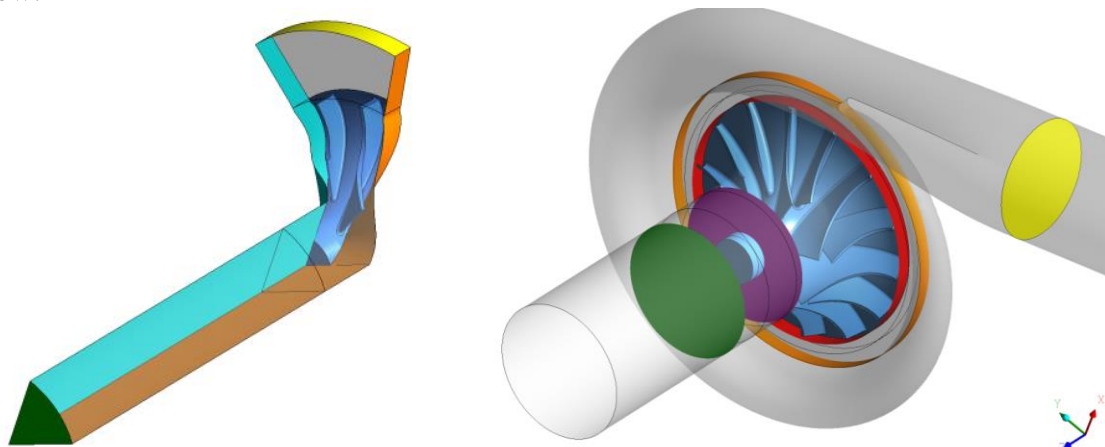


Fig. 11: Comparison of periodic flow channel model used for optimization (left) and full model used for result validation (right).

Table 7 shows the results of the validation runs normalized by the values of the reference design. The tendency, that can be seen here is the same as for the optimization results. For LC1 the performance of the optimized impeller is very similar to the reference design, whereas for LC2 a significant increase of the total pressure and the isentropic efficiency is

present. The improvement in the validation model is even bigger than predicted by the optimization model. One possible reason for this difference might be an artificial elimination of asymmetric loading of the different channels in the optimization model due to the assumption of a periodic flow. In the validation model, the asymmetry of the flow for the reference model appears to be stronger than for the optimized designs; which leads to decreased efficiency of the reference model compared to the optimized designs.

Output / Objective (term)	Reference	Design 3943	Design 144
Normalized isentropic efficiency LC1	1.00	1.04	1.03
Normalized total pressure ratio LC1	1.00	1.00	0.97
Normalized isentropic efficiency LC2	1.00	1.17	1.19
Normalized total pressure ratio LC2	1.00	1.06	1.06

Table 7: Comparison of the results of validation runs for the optimized geometries.

8 Conclusion

In this paper, the optimization of the fluid mechanical and structural properties of a radial compressor impeller, used in the so called eAC, is presented. Due to special restrictions such as limited rotational speed, limited design space and the need for fast acceleration of the eAC impeller the systematic and multiphysical approach of the numerical optimization process was estimated to be especially beneficial. The intense testing and geometry variation that took place during the course of the project enabled the stability of the KSPG Excel-tool and the connected CAE-process to be improved. Hence, the usability in a numerical optimization process could be demonstrated.

As a result of the sensitivity analysis, the six geometry parameters with the biggest influence on the important performance indicators of the compressor could be identified. The key outcome of the optimization is a significant reduction of the mass and moment of inertia of the impeller (approx. -45%). Additionally the impeller shows improved efficiency and pressure ratio near the surge line without falling back behind the conventional initial design at the design point. Last but not least, the optimized impeller design proves to be robust against statistical variation of selected input parameters based on the premise of assuming their distribution.

Comparative engine process simulations of a load step at low engine speed have been conducted for the original and the optimized compressor wheel in order to illustrate the benefits regarding the transient response of the internal combustion engine provided by the optimized eAC. Fig. 12 shows the acceleration of the eAC during the load step. Due to its reduced moment of inertia, the optimized impeller reaches its target speed in a shorter time.

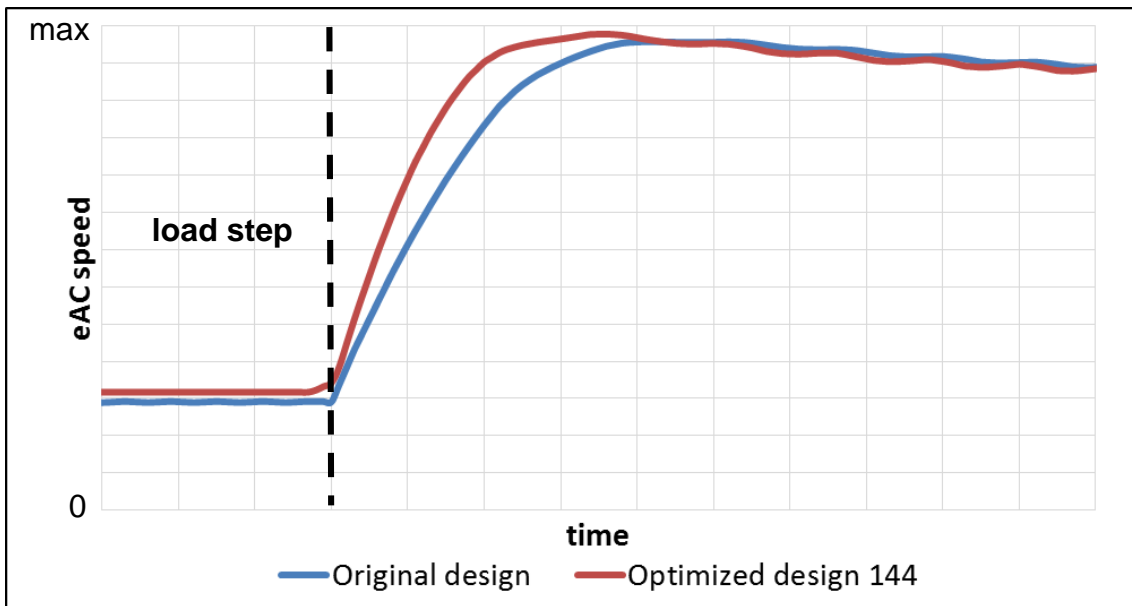


Fig. 12: Transient response of the eAC rotation rate during load step of the combustion engine.

The combination of the faster acceleration with the increased efficiency of the impeller near the surge line also allows the optimized eAC to provide a faster response of the engine to an acceleration demand coming from the driver of the vehicle, an example of which is shown in Fig. 13. Through this improvement, it is possible to demonstrate the positive impact of using numerical optimization methods on the original function of the eAC.

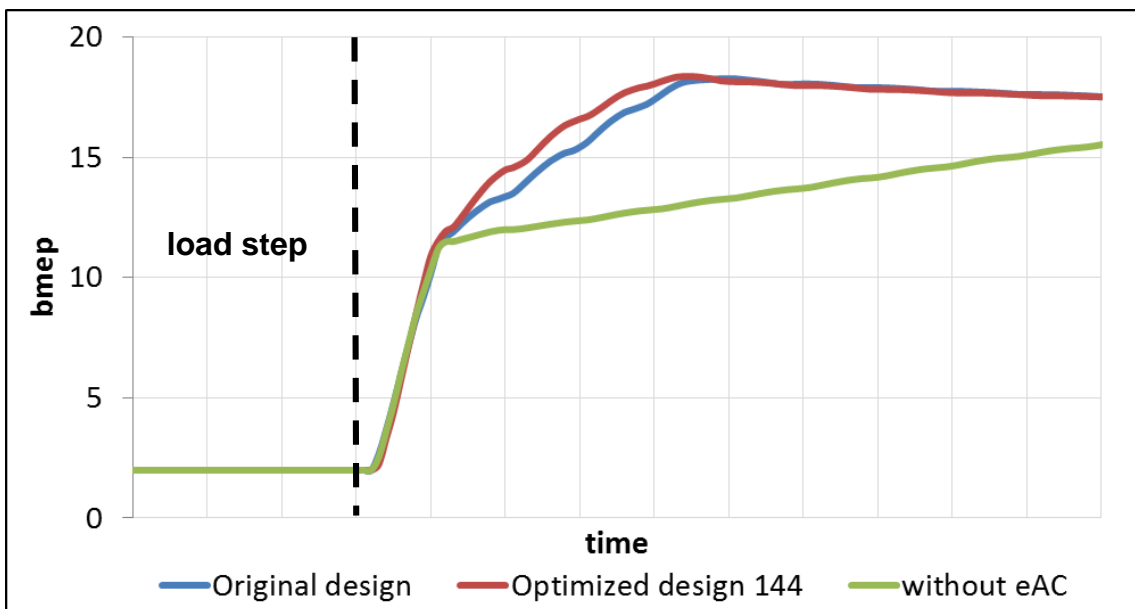


Fig. 13: Brake mean effective pressure during load step of the combustion engine.

9 References

- [1] KNIRSCH S., WEIß U., ZÜLCH S., KILGER M.: Die elektrische Aufladung im Audi RS 5 TDI Concept. In: *MTZ – Motortechnische Zeitschrift*, Issue 01/2015, Page 36-41
- [2] AUBIN S., LEFEVRE T., PRINCIVALLE R.: Improvement of a low speed – highly loaded compressor driven by an electric motor dedicated to the supercharging system of an internal combustion engine. In: *Proceedings of the 19th Supercharging Conference*, Dresden, Germany, September 2014
- [3] AYMANN S., UHLMANN T., NEBBIA C., PLUM T.: Elektrische Aufladung – Neue Freiheitsgrade durch höhere Bordnetzspannung. In: *MTZ – Motortechnische Zeitschrift*, Issue 07/2014, Page 12-19
- [4] MCKAY M.D., BECKMAN R.J., CONOVER W.J.: A Comparison of Three Methods for Selecting Values of Input Variables in the Analysis of Output from a Computer Code. In: *Technometrics (American Statistical Association)* 21 (2), May 1979, Page 239–245
- [5] CREMANNS K., ROOS D., GRASSMANN A.: Sequential vs. Multidisciplinary Coupled Optimization and Efficient Surrogate Modeling of a Last Stage and the Successive Axial-radial Diffuser in a Low Pressure Steam Turbine. In: *Proceedings of ASME. 45615; Volume 2B: Turbomachinery*, June 16, 2014
- [6] ROOS D., CREMANNS K., JASPER T.: Probability and variance-based stochastic design optimization of a radial compressor concerning fluid-structure interaction. In: *Proceedings of V International Conference on Coupled Problems in Science and Engineering (Coupled Problems 2013)*, January 2013
- [7] MOST T., WILL J.: Meta-model of Optimal Prognosis - An automatic approach for variable reduction and optimal meta-model selection. In: *Proceedings of Weimarer Optimierungs- und Stochastiktag 5 (Wost 5)*, November 2008